Permanent WRAP url:
http://wrap.warwick.ac.uk/54473

http://go.warwick.ac.uk/lib-publications

Influence of Boundary Conditions and Geometric Imperfections on Lateral-Torsional Buckling Resistance of a Pultruded FRP I-beam by FEA

T.T. Nguyen [a], T.M. Chan [a,*] and J.T. Mottram [a]

[a] School of Engineering, University of Warwick, Coventry, CV4 7AL, UK.

Abstract

Presented are results from geometric non-linear finite element analyses to examine the lateral torsional buckling (LTB) resistance of a Pultruded fibre reinforced polymer (FRP) I-beam when initial geometric imperfections associated with the LTB mode shape are introduced. A data reduction method is proposed to define the limiting buckling load and the method is used to present strength results for a range of beam slendernesses and geometric imperfections. Prior to reporting on these non-linear analyses, Eigenvalue FE analyses are used to establish the influence on resistance of changing load height or displacement boundary conditions. By comparing predictions for the beam with either FRP or steel elastic constants it is found that the former has a relatively larger effect on buckling strength with changes in load height and end warping fixity. The developed finite element modelling methodology will enable parametric studies to be performed for the development of closed form formulae that will be reliable for the design of FRP beams against LTB failure.

---
[*] Corresponding author. Tel.: +44 (0)24 765 22106; fax:+44 (0)24 76 418922
E-mail addresses: T.Nguyen-Tien@warwick.ac.uk (T.T.Nguyen), T.M.Chan@warwick.ac.uk (T.M.Chan), J.T.Mottram@warwick.ac.uk (J.T.Mottram).

Keywords: Lateral-torsional buckling; geometric non-linear finite element analysis; fibre reinforced polymer; load height; warping restraint; initial geometric imperfections.

Notation

e_y Load eccentricity displacement normal to the minor axis plane of the beam cross-section (mm)

b Breadth of I-beam (mm)

h Height of I-beam (mm)

k Restraint factor for lateral flexural bending at end supports; 0.5 for full restraint to 1.0 for fully unrestrained

k_w Restraint factor for warping at end supports; 0.5 for full restraint to 1.0 for fully unrestrained

C_1 Factor to account for the type of moment distribution and support condition

C_2 Factor to account for the vertical position of the load with respect to the shear centre (centroidal axis) of the I-beam

C_b Moment modification factor for non-uniform moment distribution for laterally unsupported span when both ends of the beam are braced

E Modulus of elasticity (kN/mm^2)

E_L Longitudinal modulus of elasticity (kN/mm^2)

E_T Transverse modulus of elasticity (kN/mm^2)

G Shear modulus (kN/mm^2)

G_{LT} In-plane shear modulus (kN/mm^2)

v Poisson's ratio (for steel)

v_{LT} Major Poisson's ratio

I_w Warping rigidity (mm^6)

I_z Second moment of area for flexure about the beam's minor axis (mm^4)

J	Torsional rigidity (mm^4)
L	Span of beam or height of column for defining magnitude of out-of-straightness (mm)
w	Vertical deflection of shear centre at mid-span (mm)
M_{cr}	Elastic critical buckling moment of resistance (kNm)
M_{crp}	Elastic critical buckling moment including the influence of pre-buckling displacements (kNm)
P	Central point load (kN)
P_{cr}	Elastic critical buckling load of simply supported beam subjected to centre point loading (kN)
$P_{cr,FEA}$	Elastic critical buckling load obtained from linear (Eigenvalue) Finite Element Analysis (kN)
P_{Limit}	Limiting buckling load (kN)
P_{Limit}/P_{cr}	Normalized buckling load for influence of geometric imperfections
$P_{cr,T}$	Elastic critical buckling load when P is applied on Top flange (kN)
$P_{cr,S}$	Elastic critical buckling load when P is applied at Shear centre (kN)
$P_{cr,B}$	Elastic critical buckling load of beam P is applied on Bottom flange (kN)
$P_{cr,Fixed}$	Elastic critical buckling load of beam with end warping fully Fixed ($k_w = 0.5$) (kN)
$P_{cr,Free}$	Elastic critical buckling load of beam with end warping fully Free ($k_w = 1.0$) (kN)
x	Distance along beam from one end the other end (mm)
z_g	Distance (height) from the shear centre to the point of load application (mm)

Δ_s	Maximum lateral deformation due to out-of-straightness geometric imperfection (mm)
Δ_{sx}	Initial lateral deformation distribution along the beam due to out-of-straightness geometric imperfection (mm)
Δ_t	Maximum angle of twist due to twist geometric imperfection (degrees)
Δ_{tx}	Initial twist distribution along the beam due to twist geometric imperfection (degrees)
U_x	Displacement in X-direction (mm)
U_y	Displacement in Y-direction (mm)
U_z	Displacement in Z-direction (mm)
U_{Rx}	Rotation about X-axis (degrees)

Introduction

Shapes and systems of Fibre Reinforced Polymer (FRP) made by the pultrusion processing method [1] are finding applications in civil engineering works, alongside construction components of conventional materials such as steel, concrete and aluminium. Standard Pultruded FRP (PFRP) shapes are thin-walled and have the same cross-sectional shapes as found in conventional steelwork. They consist of E-glass fibre reinforcement (layers of unidirectional rovings and continuous mats) in a thermoset resin based matrix. Layers are not necessarily of constant thickness or flat. Technical information on the pultrusion process, and PFRP shapes themselves, is found in American pultruders' Design Manuals [2, 3]. Pultruded material has a density at 1900 kg/m^3 that is under one-quarter the density of structural steel. Although these PFRP shapes are similar to steel sections, their structural behaviour is different. Direct strengths (in the direction of pultrusion) can be over 200 N/mm^2 that is comparable with structural steel. However, the longitudinal (tensile or compressive) modulus of elasticity (E_L) is up to 10 times lower at 20-30 kN/mm^2. The modulus of elasticity perpendicular to the direction of pultrusion (E_T) is about one-third of the longitudinal value [2, 3]. The in-plane shear modulus (G_{LT}) can be between one-tenth and one-quarter of the value of E_L. In terms of the material response to direct stress under static loading, it is virtually linear elastic to failure and can be taken as linear elastic under shear to the shear strains experienced in practice. If loading is over the long-term the viscoelastic nature of FRP will make the material response non-linear. Worldwide the number of engineering structures using pultruded standard shapes has increased in recent years, for the reasons given in Mottram [1] and Bank [4].

6

A major factor preventing greater penetration of standard PFRP shapes in civil engineering works is the lack of recognised guidelines for practitioners to have full confidence in their structural designs, say, for framed structures. One source of guidance is from the pultrusion companies who have Design Manuals [2, 3] specific to their range of pultruded shapes. Further guidance, that has no legal standing, can be found in the 1996 EUROCOMP Design Code and Handbook [5] and the more recent Italian publication [6] that is a guide for the design and construction of structures made of FRP pultruded elements. The Pultrusion Industry Council of the American Composites Manufacturers Association commenced an action, in 2007, of preparing a design standard for the 'Load and Resistance Factor Design of Pultruded Fibre-Reinforced Polymer Structures' [7]. A pre-standard was finalised in 2010, and it is expected that the guidelines can be adopted in 2013 as a national ASCE standard. To have confidence in the resistance formulae in a design standard it is desirable to have them evaluated by a combination of computational modelling and physical testing.

Owing to high strength-to-stiffness ratio of the material, the design of PFRP members (in braced frames of simple construction) is normally governed by elastic deflections and/or elastic buckling instabilities and rarely by material strength limitations [5, 8]. In other words, to execute the Ultimate Limit State (ULS) design approach the different instability modes must be quantified by a combination of rigorous numerical analysis and physical testing. As a type of global instability, Lateral-Torsional Buckling (LTB) is commonly observed in laterally unrestrained beams of open thin-walled sections that are subjected to flexure about their major axis. The beam loses stability in the LTB mode when the member bends laterally and twists along its length, without any cross-section distortion. Because a beam's moment of resistance to LTB is influenced by

having relatively small lateral (minor-axis) flexure and torsional stiffness, it is observed that PFRP I-shapes are susceptible to this failure mode governing in ULS design [9].

Researchers can determine LTB resistance, either by a theoretical treatment (analytical or computational) or by physical testing. Because the latter approach is expensive and technically challenging, for the reasons that are uncovered from assessing the reported test series [9-13], a theoretical treatment is always required to populate parameters that cannot be characterised by physical testing [13-15].

Numerical models can be divided into those that account for geometric imperfections and those that assume the beam's geometry is perfect. It is the analytical solutions for the problem of a 'perfect' isotropic beam with constant moment along length that gives the well-known closed form formula for the elastic critical buckling moment of resistance (M_{cr}). This M_{cr} solution is the theoretical upper bound resistance that forms the basic strength value towards the preparation of guidelines for the reliable and safe design of structural steel I-beams, as given in design standards BS EN 1993-1-1:2005 and ANSI/AISC 360-10.

For doubly symmetric cross-sectional (steel) beams, the lateral-torsional buckling resistance moment may be calculated using [16]:

$$M_{cr} = C_1 \frac{\pi^2 E I_z}{(kL)^2} \left\{ \sqrt{\left(\frac{k}{k_w}\right)^2 \frac{I_w}{I_z} + \frac{(kL)^2 GJ}{\pi^2 E I_z} + \left(C_2 z_g\right)^2} - C_2 z_g \right\} \tag{1}$$

The variables in Equation (1) are defined in the Notation section. This equation can be used to determine M_{cr} when calculating LTB resistance in accordance with the design procedure in Eurocode 3 for steel (BS EN 1993-1-1:2005).

In the specific case, when loading is a vertical point load (P) at mid-span, and beam ends are free to warp ($k_w = 1.0$) and allowed to rotate about major and minor axes ($k = 1.0$), the buckling resistance load P_{cr} is given by:

$$P_{cr} = \frac{5.39\pi^2 EI_z}{L^3}\left\{\sqrt{\frac{I_w}{I_z} + \frac{L^2 GJ}{\pi^2 EI_z} + \left(0.63 z_g\right)^2} - 0.63 z_g\right\} \tag{2}$$

In Equation (2) z_g is the height of the load from the shear centre. z_g is 0.0 at the shear centre and positive when above and negative when below.

According to American steel standard ANSI/AISC 360-10 M_{cr} may also be determined for I-beams from the simpler formula:

$$M_{cr} = C_b \frac{\pi}{L}\sqrt{\frac{I_w}{I_z} + \frac{L^2 GJ}{\pi^2 EI_z}} \tag{3}$$

Unlike Equations (1) and (2), Equation (3) is valid only when the level of loading coincides with the beam's shear centre (i.e. for z_g is zero).

Italian guidelines of 2007 [6] recommend that M_{cr} be calculated using Equation (1) with both restraint factors k and k_w equal to either 1.0 or 0.5. The Design Manuals from two American pultruders [2, 3] recommend that designers calculate M_{cr} using Equation (1), with k and k_w assumed to be equal to 1.0 (for the lowest LTB moment of resistance). Moreover because they take $z_g = 0.0$, the allowable load tables in [2] and [3] are ignoring the reduction in strength from having load applied on the top flange. Reliable calculation of the elastic critical buckling strength does require the two elastic constants E_L and G_{LT} to be measured, either by testing coupons or full-sections [4].

The American pre-standard for PFRP structures [7] recommends M_{cr} to be calculated using Equation (3), with the expression for C_b formula taken directly from ANSI/AISC 360-10, and with the 'full-section' elastic constants of E and G replaced, respectively, by the Longitudinal modulus of elasticity E_L and the in-plane shear modulus G_{LT} for the PFRP material.

The aim of the work reported in this paper is to use Finite Element Analysis (FEA) to study the change in LTB resistance of a, single sized, PFRP I-beam at different spans that is influenced by varying load height, end displacement boundary conditions and initial geometric imperfections. The shape is chosen from the standard range of I-beams pultruded in America [2, 3]. To be consistent with the set-up in a series of physical tests at the University of Warwick, the problem analysed, using ABAQUS®, is that of a simply supported beam (for Major axis flexure) having a vertical point load at mid-span. Verification of the correct FE modelling methodology to simulate what can exist in practice will be done by combining results from the experimental and finite element work. Additional numerical results from FEA will be used with Equation (2) and the 'curve fitting' method of Dutheil [17] to account for the modal interaction of local and global buckling modes [18,19], to prepare a calibrated closed form formula for clauses in a future Eurocode design standard for FRP material elements.

To ensure the FEA results are appropriate when the beam possesses initial geometric imperfections it is necessary to use the geometric non-linear solver in ABAQUS®. It will be shown that the calculated vertical load against vertical deflection response of a PFRP beam does not always give a distinct buckling (bifurcation) point to signal the onset of LTB failure. To overcome the absence in numerical calculations of a definite

elastic critical buckling load (for the classical bifurcation point) a data reduction method is presented by the authors that will provide the limiting buckling load from the finite element (FE) results.

Finite element modelling methodology

In this study the nominal geometry of the cross-section for the PFRP I-beam is 101.6 ×50.8×6.4 mm (or 4×2×1/4 in. [2, 3]). The height has the notation h, which is used to define beam slenderness through non-dimensional ratio L/h. In Figure 1 the global Cartesian (XYZ) co-ordinate system is shown. The Y-axis is for the section's major axis, the Z-axis is for the minor axis and the X-axis is along the beam's centroidal axis. The nominal values for the sectional properties are: I_z is 1.41×10^5 mm^4, I_w is 3.16×10^8 mm^6 and J is 1.59×10^4 mm^4. These are required later when Equation (2) is used to calculate the elastic critical buckling load, P_{cr}. The flanges and web panels are given orthotropic properties, defined by the four elastic constants of E_L, E_T, G_{LT} and ν_{LT} [5, 10]. ABAQUS® [20] offers several options to input mechanical properties including: a 'microscopic' approach (micromechanical modelling requiring constituent matrix and fibre reinforcement properties); a 'macroscopic' approach (where a layer or panel is taken to be a single orthotropic material); a 'mixed' approach (the panel is modelled as a lamination comprising a number of discrete 'macroscopic' orthotropic layers). Because the four elastic constants have previously been determined by coupon testing and micro-mechanical modelling [19, 21] the 'macroscopic' approach is appropriate for this FE work.

It is observed that mechanical properties of PFRP shapes can change with pultruder. This change is due to differences in: how a property is measured; processing conditions;

the matrix; the number of reinforcement layers; the fibre arrangement and the fibre volume fractions. To illustrate the likely differences, Table 1 collates test data for the in-plane shear modulus (G_{LT}). Listed in column (2) are ranges of values taken from the nine sources defined in column (1). Shear modulus is difficult to measure because it is challenging to have a representative volume of PFRP material subject to pure shearing. Using knowledge of measurements of the elastic constants and the findings of the review by Mottram [28], for the determination of in-plane shear modulus, engineering judgement has been used to establish that, for this FE work, E_L is 24 kN/mm^2, E_T is 8 kN/mm^2, G_{LT} is 4 kN/mm^2 and ν_{LT} is 0.3. It is noted from the literature that the mechanical properties of flange and web material are actually slightly different. Since flanges and web thin-walled panels are assumed to be of the same orthotropic material, any influence this secondary difference might have on FE result has been ignored. Moreover, E_L and E_T are for direct tension (or direct compression) and, because of the layered construction, are not the moduli if the panel is subjected to flexure. By correctly assuming that the material response is linear elastic to a strain that will exceed the strain at LTB failure, the FEA does not need to consider a material failure criterion. Moreover, the influence, if any, of residual stresses throughout the cross-section, which are unknown in pultruded FRP shapes, is neglected too.

The choice of element to create a mesh is between solid and shell types of elements. Linear elastic flat shell elements have successfully been adopted in previous FE studies with thin-walled FRP structures [10, 12, 29, 30]. The element chosen is the second-order ABAQUS®/Standard thick shell element S8R, having 8-nodes and six degrees of freedom per node. The formulation for the element stiffness matrix adopts the Mindlin plate theory (for first-order shear deformation) and so this thick shell element has

displacement compatibility that avoids there being any discontinuities between element sides. This FE modelling attributes is known to give a more accurate shell element in a coarser mesh [31].

Following the boundary conditions defined by Trahair [32] for a simply supported beam, both ends are fully restrained for Y and Z translational displacements (U_y and U_z) and rotation about the X-axis (U_{Rx}). Ends are free to rotate about major and minor axes (for $k = 1.0$) and allowed freely warp ($k_w = 1.0$). Because effective length factors k and k_w may vary from 0.5 to 1.0, a parametric study could consider a number of distinct displacement boundary conditions. FEA results will be presented later for the two end conditions of either having both k and $k_w = 1.0$, or having $k = 1.0$ and $k_w = 0.5$. In what follows these two displacement boundary conditions are given labels BC1 and BC2.

BC1 is specified in the FE modelling by setting $U_y = U_z = U_{Rx} = 0$ for all the nodes in the cross-section, at both ends. At one end, the node located at the cross-section's shear centre has its U_x nodal displacement set to zero to remove a rigid-body movement. To model the BC2 end condition the ends are fixed against warping. As Figure 1 shows a vertical plate, comprising of R3D4 rigid surface elements, is added at the ends. Because the beam flanges must deform in accordance with the movement of the 'rigid' plate this modelling feature fully restrains the warping. As the movement of the rigid plate is controlled by a single reference node at each end, translational and rotational displacement restraints are imposed to the node at the I-beam's centroid. Figure 1 shows that to obtain BC2 one end requires this node have $U_x = U_y = U_z = U_{Rx} = 0$, while at the other end the equivalent node has $U_y = U_z = U_{Rx} = 0$.

Mesh specification has the shell elements constructed with an aspect ratio close to one, as this can eliminate any loss in numerical reliability due to computation for the inclusion of shear flexibility. To create the beam's mesh the shell elements are placed at the mid-planes of the two flanges and web panels. Equally spaced, there are five nodes (four shell elements) across the 50.8 mm flange width and nine nodes (eight elements) over the web's height of 95.6 mm. This mesh specification gives an element with side lengths of 12.7 by 12.7 mm for flanges and 11.9 by 12.7 mm for web. As shown in Figure 1 one metre length of the 101.6×50.8×6.4 mm I-shape requires 1108 elements.

Table 2 reports the elastic critical buckling load ($P_{cr,FEA}$) as the mesh size is refined. These FE results are from Eigenvalue analyses with a perfectly straight beam, BC1 end conditions and shear centre point load (P) at mid-span. It can be seen that there is insignificant change in $P_{cr,FEA}$ when the element side length is < 12.7 mm. However, it is seen that on doubling the side length to 25.4 mm the calculated bifurcation load is increased by 10%. Shell elements with side lengths of 12.7 mm or less are used in the mesh specification for the FE results presented next.

The parametric studies have numerical simulations for both linear Eigenvalue analyses and geometric non-linear analyses. Eigenvalue buckling analysis predicts the elastic critical buckling load ($P_{cr,FEA}$) of a linear elastic beam where the change in beam geometry is neglected on increasing loading, up to the bifurcation. By applying perturbations to the mesh geometry of the unloaded beam, and looking for local and global deflections that could promote the onset of instability due to second-order effects, the FEA gives load factors (the Eigenvalues) for buckling failures. The inputted load in the FE model is multiplied by the outputted load factor to obtain the elastic critical buckling load. The associated eigenvector to each Eigenvalue establishes the

corresponding mode shape. The mode shape describes how the structure buckles, but gives no information for actual load-deflection response. It can be expected that the lowest Eigenvalue is for the mode having the lowest $P_{cr,FEA}$.

In contrast, a non-linear geometric analysis predicts the actual load-deflection response by applying the load in small increments and evaluating the current (static equilibrium) deformation state at each increment. The load follows the deformation of the linear elastic beam until instability occurs, and this corresponds to what will happen in practice. There is no material non-linearity as it is assumed the PFRP material behaves perfectly linear elastic. This modelling assumption is acceptable, providing loading (to failure) is short-term and deformations from material viscoelasticity remain small. ABAQUS® [33] will solve the problem of a geometric non-linear structural problem, having a falling load-deflection branch, following instability failure, by employing a modified Riks method. This commonly used non-linear numerical method, also known as the arc-length method, was originally derived by Riks [34], following on from pioneering work by Wempner [35]. Later the arc length method was improved for computational efficiency by Crisfield [36].

As the post-buckling response is not the main topic under consideration, the Riks analysis was terminated a few increments after the beam had become unstable and its deformation was progressing into the post-buckling region.

Initial geometric imperfection is introduced into the beam's FE mesh by modifying the nodal coordinates through the adoption of a vector field. The out-of-straightness imperfection was obtained by scaling the first Eigenvalue buckling mode shape for Euler (flexural) buckling of a perfectly straight concentrically loaded column. The

deformed shape (exaggerated) from the Eigenvalue analysis is shown in Figure 2. The geometric definition for the twist imperfection was acquired from the deformed shape of an 'imperfection-free' beam subjected to a pure 'twisting' moment, that was generated by a torque at the free end, created by applying there a couple of magnitude *Pb* (Figure 3). The static analysis deformation for twisting along the length of the I-shape is shown in Figure 4.

Influence of load height

LTB resistance is influenced by the vertical distances of load (z_g) from the shear centre due to the additional torque about the longitudinal (centroidal) axis that is generated from the lateral movement of the vertical point load when instability happens. Because the torque acts in the opposite sense to the LTB twist rotation when the load is applied below the shear centre the buckling resistance will increase. Likewise, when load acts above the shear centre, the additional torque acts with the beam's rotation to decrease buckling resistance. This behaviour has been confirmed by Sapkás and Kollár [37] and Machado and Cortínez [38] in their numerical studies on the same instability mode of failure.

In this study, the effect on resistance of changing load height z_g is established by Eigenvalue analyses that obtain the bifurcation load with displacement boundary conditions BC1. The span (*L*) varies from 1.0 to 5.0 m; which is for slenderness (*L/h*) ratios from about 10 to 50. In the FE model the mid-span point load is positioned along the Z-Z axis at the top flange and web junction ($z_g = 47.6$ mm), shear centre ($z_g = 0.0$ mm) and at bottom flange and web junction ($z_g = -47.6$ mm). Note that these values of z_g are 3.2 mm below what they will be when the actual beam section is loaded. By

changing the elastic constants to those for structural steel (E is 210 kN/mm^2 and ν is 0.3) the effect on $P_{cr,FEA}$ for a beam of this isotropic material is established. To distinguish between the $P_{cr,FEA}$s for the three load heights they are given the notation $P_{cr,T}$, $P_{cr,B}$ and $P_{cr,S}$ for load at Top flange, at Shear centre and at Bottom flange, respectively. The subscript FEA has been removed from the notation for these three critical elastic buckling loads.

Plotted in Figure 5 are LTB load ratios $P_{cr,T}/P_{cr,S}$ and $P_{cr,B}/P_{cr,S}$ against slenderness for the beam of either FRP or steel. It is obvious that for the same beam configuration, the closer the buckling load ratios are to 1.0, the less significant is the load height influence. The higher $P_{cr,B}/P_{cr,S}$ is, and the lower $P_{cr,T}/P_{cr,S}$ is for PFRP compare to steel shows that the change of load height is more significant for the composite material. The maximum difference between the steel and PFRP curves is 11% at the lowest slenderness ratio of 9.8, and the minimum difference is 4%, when L/h is 49.2.

Plotted in Figure 6 is the normalized LTB load $P_{cr,FEA}/P_{cr}$ versus L/h for the PFRP beam. P_{cr} was calculated using Equation (2). Because the normalised load does not deviate significantly from 1.0, the three curves in the figure confirm that Equation (2) gives $P_{cr,FEA}$s similar to those from the Eigenvalue FEA with the same parameter values. When slenderness L/h is < 15 the reliability of Equation (2) in predicting LTB resistance is seen to decrease.

Figure 7 is for plots of mid-span vertical point load (P) with mid-span vertical deflection (w) for a virtually straight beam. The beam has a span of 2 m and the out-of-straightness geometric imperfection has maximum amplitude of span/20000. From the three load-deflection curves in the figure it can be seen that $P_{cr,FEA}$ (for the onset of LTB

failure) depends on z_g. Instability happens when the beam's vertical stiffness (P/w) dramatically reduces. It is observed that until the instability starts to develop, the three P-w curves are identical, and so initial vertical stiffness is not influenced by the load height. Mohri *et al*. [39] recorded a similar observation when analyzing the buckling behaviour of steel beams. It is also worth noting that, from a designer's point of view, when the load is applied below shear centre (i.e. z_g is negative), the governing limit state for the PFRP beam section can be a serviceability deflection limit.

Influence of end warping fixity

When a thin-walled cross-section has an open shape its stiffness under torsion, acting about the centroidal axis, is the sum of torsional stiffnesses from uniform (St. Venant) torsion (governed by torsional rigidity $G_{LT}J$ or GJ) and from non-uniform torsion (controlled by warping rigidity $E_L I_w$ or $E I_w$). When the ends of the beam have warping fully fixed the state of non-uniform torsion will be dominant and because the stiffness to twisting deformation increases, so does the resistance to LTB failure. On the other hand if warping at the ends is free, the state of non-uniform torsion reduces (it will be present either side of the mid-span when a torque is generated by P) and the LTB resistance is the lower bound for this end displacement boundary condition. It is because the free warping condition is for lowest strength that k_w is specified to be 1.0 in design, such as given by the closed form Equations (2) and (3). Minghini *et al*. [40] investigated by analysis the critical load of a PFRP portal frame, where the column ends were either free warping or fully warping fixity. They found that there was a 40% increase in buckling load between these two bounds on a displacement boundary condition.

Plotted in Figure 8 is the ratio of elastic critical buckling loads with BC2 for end warping fully restrained ($P_{cr,Fixed}$) and BC1 for warping fully free ($P_{cr,Free}$), for slenderness ratios from 9.8 to 49.2. For convenience the subscript FEA has been removed from these two FE Eigenvalue solutions. The top curve is for FRP and the lower curve is for steel elastic constants. It is noted that the contribution of non-uniform torsion stiffness to the total torsional stiffness (defined by $E_L I_w / (E_L I_w + G_{LT} J)$ or $E I_w / (E I_w + G J)$) is bigger for FRP, and so the effect of changing the warping restraint from free to fixed is greater for the same beam geometry and displacement and loading boundary conditions. It can be seen from the figure that $P_{cr,Fixed}/P_{cr,Free}$ for FRP varies from 1.13 to 1.66 and for steel from 1.07 to 1.48. The maximum difference between steel and FRP is 13%, when L/h is 14.8. The minimum difference of 4.3% is found to be at the slenderness ratio of 44.3.

It is well-known [32] that the effect of warping torsion reduces as the span gets longer, such that its influence on buckling resistance reduces too. As the contribution of warping torsion (on total torsion) is highest with end warping fixed, the reduction in buckling resistance is biggest when $k_w = 0.5$. As consequence the ratio $P_{cr,Fixed}/P_{cr,Free}$ is higher for stockier beams. The result of interaction of the two torsional stiffnesses on LTB strength is seen from the curves plotted in Figure 8.

Influence of initial geometric imperfections

In this study only the influence of expected manufacturing imperfections on the geometry of the PFRP I-shape are considered in a FE parametric study. Another 'imperfection' that is inherent will be the eccentricity of load from having the vertical load offset a distance, e_y, from the Z-Xplane. This imperfection introduces a 'secondary'

moment of magnitude Pe_y that will either act with, or against the beam deformation induced by the presence of geometric imperfections [41]. In other words the presence of a larger geometric imperfection can be employed to account for the load eccentricity that is due to tolerances found on on-site or in laboratory testing. As a result this particular form of imperfection is not included in the FE modelling. Structural PFRP shapes are pultruded to possess acceptable geometric imperfections in the form of out-of-straightness, flatness, twist, angularity, etc. It is imperative to include these geometric imperfections in the FE modelling methodology as their existence in practice will lower the LTB buckling resistance. It could be argued that an acceptable approach in FEA is to scope geometric imperfections, residual stresses and load eccentricity by modelling the dominant type of imperfection with a relatively high magnitude. Investigated next is the influence on LTB resistance of changing the two key geometric imperfections of minor axis out-of-straightness and (longitudinal) twist. These two geometric imperfections are directly linked to the two (governing) LTB deformations of lateral flexural and cross-section twist, respectively.

The question to next address is how large are the two geometric imperfections to be? Maximum allowable magnitudes can be based on ASTM D3917-11 for Standard Specification for Dimensional Tolerance of Thermosetting Glass-Reinforced Plastic Pultruded Shapes [42]. Table 3 reports information taken from Tables 3 and 4 in ASTM D3917-11 to give the 'allowable deviation from straight' per unit length. Column (1) lists the type of imperfection and column (2) provides an illustration. In column (3) the values of the allowable deviation from straightness (Δ_s) or twist (Δ_T) is reproduced. The standard has made the assumption that the initial lateral out-of-straightness (Δ_{sx}), along a beam of length L, to be defined by the geometric relationship

$$\Delta_{sx} = \Delta_s \sin \frac{\pi x}{L} \quad .$$

(5)

For the initial twist imperfection the assumed distribution along the length is given by

$$\Delta_{tx} = \Delta_t \sin \frac{\pi x}{2L} \quad .$$

(6)

In Equations (5) and (6) x is the distance along the beam from one end to the other end.

It is noted that the maximum twisting allowance in 2011 version of ASTM D3917 is three times larger than in the previous version of 2002. The reason for this significant change has not been given provenance by the drafting committee. A maximum limit on the twist angle is not given in ASTM D3917-11; it was stated to be 3 degrees in 2002.

Table 4 reports measured values for the magnitude of geometric imperfections, in terms of L, for a range of standard pultruded standard shapes [2, 3]. In column (1) the source to the data is given. Column (2) gives the form of shapes characterised by an 'in-house' measurement method of the research centre, and results are listed in column (3). It is noted that no measurements for the twist imperfection have been made. Table 4 reports that the minor axis out-of-straight straightness imperfection (Δ_s in Equation (5)) can have a magnitude in the range of $L/800$ to $L/4500$. These measurements are found to be significantly lower than the maximum allowed in ASTM D3917-11 of $L/240$.

Figure 9 presents plots of P against w for the FRP beam at 2 m span for three initial minor axis out-of-straightnesses in the range of $L/10000$ to $L/240$. The smallest is for a virtually straight beam and the largest corresponds to the maximum allowed in manufacture. For the non-linear FEA the three-point bending load case has the displacement boundary conditions BC1 (for free warping and free lateral flexure at both

ends). Note that inspection of the deformation shape of the beams analysed did not find any signs for the development of a local instability near the sections with a shear force concentration. The three curves plotted in the figure show that, as the geometric imperfection increases, the load for LTB failure become less distinct. This FE buckling load is not the critical load it is a limiting value (P_{Limit}). It is seen from the P-w curves in Figure 9 that with the FRP material remaining linear elastic in the post-buckling region, the secondary load path has a positive slope. The curves show that, following instability, the beam develops post-buckling strength and so onset of LTB instability does not result in member collapse. This is an important finding when developing guidelines to design against LTB failure as a ULS, as its presence is analogous to the additional reliability given to design provisions in BE EN 1993-1-1:2005 and ANSI/AISC 360-10 from having the ultimate strength of steel higher than yield strength; the lower (yield) strength is used in the design calculations for LTB resistance.

Focusing on the shape of the three P-w curves in Figure 9, when P is close to 2.5 kN and w is about 10 mm, it is observed that there is no clear buckling bifurcation (for $P_{\text{cr,FEA}}$) when the out-of-straightness is L/1000 and larger. Singer et al. [44] explains that there are a number of data reduction methods that can be employed to estimate what the limiting buckling load (P_{Limit}) is. A review of methods previously employed by researchers studying pultruded shapes is given next. Lee [45], in his PhD work on the flexural-torsional buckling of T-sections, suggested that buckling load should be estimated by the intersection point of extrapolating the two 'linear' lines for the 'pre-buckling' and 'post-buckling' parts to the P-w response. In his LTB experiments with I-beams, Stoddard [12] choose to define the limiting buckling load to be the load when the mid-span rotation (twist) of the top flange attained 5 degrees. To determine the LTB

resistance of an end-loaded cantilever beam Brooks and Turvey [10] recorded their buckling load as the load at which the end-rotation started to grow rapidly. In a series of tests to determine flexural buckling of concentrically loaded columns Mottram *et al.* [41] terminated an increase to axial load when the mid-span lateral deflection reached height/100. Using measurements for column load and lateral mid-span deflection they employed the Southwell plot method to get an improved estimate to the elastic critical buckling load. Based on results from non-linear FE analyses with ANSYS®, Afifi [46] obtained column buckling loads by applying the Southwell plot method. This is known [44] to be an effective data reduction method when estimation to the elastic critical buckling load, for the perfect member, is required.

Returning to the FE results in Figure 9 it is seen that the beam's stiffness, given by P/w, is very similar during pre-buckling. The load and deflection when non-linearity occurs is dependent on the amplitude of the out-of-straightness geometric imperfection. Using these observations, the authors define the limiting buckling load P_{Limit} as the point on the load-deflection curve when the secant stiffness has been reduced by X%. Figure 10 illustrates how P_{Limit} can be obtained using this stiffness reduction method. As can be seen the initial constant stiffness is common to establishing P_{Limit} for the two non-linear P-w curves that give a lower prediction as the size of the geometric imperfections increases.

The question is, how large a percentage is X to be? To establish the answer it will be prudent to determine P_{Limit} at or near the point where the secant stiffness is changing rapidly with a small increase in w. For the 2 m beam with initial out-of-straightness of $L/10000$, Table 5 presents, in columns (1) to (3), the values of P, w and the instantaneous secant stiffness P/w. For this virtually straight beam the results show that

the 'pre-buckling' stiffness is constant at 0.262 kN/mm to P up to 2.31 kN. Secant stiffness is then found to start reducing and can be seen to be very rapidly falling away when P is 2.47 kN. At this load the 'post-buckling' stiffness is 0.138 kN/mm (highlighted in **bold font**), giving a secant stiffness reduction of around 50%. Based on this evaluation P_{Limit} is determined as the value of P when the secant stiffness reduction X is 50%.

Taking a constant 1.0 m span the FRP beam is analysed with either out-of-straightnesses of $L/10000$, $L/1000$, $L/500$ and $L/240$ or twists of 0.1^{o}, 1°, 2° and 3.28^{o}. Note that $L/240$ and 3.28^{o} are the maximum allowable in accordance with ASTM 3917-11 (refer to Table 3). Presented in Figure 11 is P_{Limit}, presented as a load ratio in terms of P_{cr} from using Equation (2). FE modelling has boundary conditions BC1 and shear centre load ($z_{\text{g}} = 0.0$ mm). For the parameters chosen $P_{\text{Limit}}/P_{\text{cr}}$ lies between 0.95 to 1.05 for the full range of the minor axis out-of-straightness and from 1.01 to 1.05 for the potential range in the twist imperfection.

The FE results in Figure 12 are for a constant out-of-straightness of $L/1000$ and a constant initial twist of 1°. It is believed that these geometric deviations are likely to be typical for pultruded I-shapes. The parameter changed in the FE study is the span, which varies from 1.0 m (L/h of 9.84) to 4.0 m (L/h of 39.4). Ratio $P_{\text{Limit}}/P_{\text{cr}}$ is seen to lie within the range of 1.02 to 1.08. Being always > 1.0, the results show that P_{Limit} is higher than that calculated by Equation (2). A feasible explanation for why the limiting value is found to be higher is that the closed form formula ignores the increase in instability resistance due to beam curvature [32]. Robert [47] found this influence is significant giving 4% increase with narrow-flange beam (i.e. height twice the flange

breadth). If this influence factor is taken into account, the buckling resistance can be determined as [46]:

$$M_{crp} = \frac{M_{cr}}{\sqrt{1 - \dfrac{I_z}{I_y}}} \qquad (4)$$

For the single beam section in this FE study Equation (4) gives $M_{crp} = 1.04 M_{cr}$. This means that a resistance increase of 4% can be from the pre-buckling deformation.

It is also observed that P_{Limit}/P_{cr}, for 'slender' beams with $L/h > 20$, is fairly constant at 1.07 to 1.10. When the beam becomes 'stocky' (with slenderness ratio < 15), P_{Limit}/P_{cr} is now found to be in range 1.02 to 1.05. The transition in buckling resistance can be explained by the presence of a growing contribution from shear deformation as the beam gets shorter. The model for the development of Equation (2) does not account for shear flexibility.

Concluding remarks

Linear Eigenvalue and geometric non-linear Finite Element (FE) analyses have been performed to study the Lateral-Torsional Buckling (LTB) resistance of the I-beam (of size 101.6×50.8×6.4 mm) under the influence of load height, displacement boundary conditions and the geometric imperfections of minor axis out-of-straightness and longitudinal twist. It is found that changing the load height relative to the shear centre is more significant for a beam of Pultruded Fibre Reinforced Polymer (PFRP) than of structural steel. It is found that the change in resistance is significant when the beam is 'stockier', as given by span/height ratio < 15. When the Eigenvalue results are normalized using the prediction for the elastic critical buckling load from a closed form

25

formula it is found that the ratio remains close to 1.0 (between 0.94 and 1.02). The FE study on influence of load height with the PFRP beam does show that the post-buckling load path is significantly affected by this parameter.

By studying the influence of the degree of end warping fixity on LTB resistance it is found to be more significant when the beam is of FRP material. The level of influence is reduced as the beam span increases and an explanation for the finding is developed in the paper.

To simulate pre-buckling response in the presence of geometric imperfections, emanating during the pultrusion process, it is necessary to perform a geometric non-linear analysis. It is found that the vertical load against vertical deflection curve does not show a clear buckling (bifurcation) point for LTB failure. A data reduction method is proposed to allow an acceptable prediction of the limiting buckling load. It is given by the point on the load-deflection curve at which the secant stiffness has reduced by 50% from its initial constant value. By adopting this method, limiting buckling loads are obtained for a 1.0 m long FRP beam having initial geometric imperfections of out-of-straightness from span/10000 to span/240 and twist along span from 0.1^{o} to 3.28^{o}. Normalized buckling load is shown to be in the range of 0.95 to 1.05 and 1.01 to 1.05, respectively. A value of 1.0 means the FE result is identical to that from a closed form equation developed for the design of isotropic (steel) members in bending. By setting the two imperfections constant at span/1000 and 1° the buckling load ratio, from increasing spans from 1.0 to 4.0 m, is found to be 1.03 to 1.08 and 1.04 to 1.1, respectively. The lowest ratios are for slenderness ratio < 15 and can be explained by the growing influence of shear deformation. The physical explanation for why the FE

results for the FRP I-beam are above that calculated by the closed form equation is given.

The authors recommend their FE modelling methodology for PFRP beam problems with geometric imperfection failing with the lateral-torsional buckling mode.

For the development and calibration of a closed form formula for inclusion in a design standard other geometric imperfections such as flatness, angularity and residual stress might have an important role to play in reducing LTB resistance. Based on the relevance of the results from the work reported in this paper the authors believe that the inclusion of all 'field' imperfections can be scoped by modelling a single (dominant) imperfection with appropriate magnitude. The most practical to work with is that of out-of-straightness about the minor-axis, having maximum amplitude of, say, span/200.

Reference

1. Mottram JT. Does Performance Based Design with Fibre Reinforced Polymer Components and Structures Provide any New Benefits and Challenges?. The Structural Engineer 2011;89(6):23-27.
2. Anonymous. Strongwell Design Manual. Strongwell Composites Inc, Bristol, VA. (www.strongwell.com/) (1st August 2012).

3. Anonynous. The New and Improved Pultrex Pultrusion Design Manual (Imperial version) Vol. 4 Rev. 6. Creative Pultrusion Inc., Alum Bank, PA. (www.creativepultrusions.com/library.html) (1st August 2012).

4. Bank LC. Composites for Construction - Structural Design with FRP Material. John Wiley & Sons, New Jersey 2006.

5. Clarke JL (Ed.). Structural Design of Polymer Composites: Eurocomp Design Code and Handbook. S & FN Spon, London 1996.

6. Anonynous. Guide for the Design and Construction of Structures made of Thin FRP Pultruded Elements. National Research Council of Italy (CNR), Rome, Italy, 2008. (http://www.cnr.it/documenti/norme/IstruzioniCNR_DT205_2007_eng.pdf) (1st November 2012)

7. Anonymous. Pre-Standard for Load and Resistance Factor Design (LRFD) of Pultruded Fiber Reinforced Polymer (FRP) Structures. American Composites manufacturers Association (ACMA), Arlington, VA. press release. (www.acmanet.org/pressreleases/2011/011711.html) (1st August 2012).

8. Chambers RE. ASCE Design Standard for Pultruded Fiber-Reinforced-Plastic (FRP) Structures. Journal of Composites for Construction 1997;1(1): 26-38.

9. Mottram JT. Lateral-torsional Buckling of a Pultruded I-beam. Composites 1992;23(2): 81-92.

10. Brooks RJ, Turvey GJ. Lateral Buckling of Pultruded GRP I-section Cantilevers. Composite Structures 1995;32(1-4): 203-215.

11. Turvey GJ. Effects of Load Position on the Lateral Buckling Response of Pultruded GRP Cantilevers - Comparisons Between Theory and Experiment. Composite Structures 1996;35(1): 33-47.

12. Stoddard WP. Lateral-torsional Buckling Behavior of Polymer Composite I-shaped Members. PhD Thesis, Georgia Institute of Technology, Atlanta, Georgia 1997.

13. Trumpf H. Local and Global Stability of Plane Frame Works made of Orthotropic FRP-profiles. PhD thesis, University of Aachen, Germany, Shaker-Verlag 2006.

14. Zhang S. Lateral-torsional Buckling of Simply Supported and Cantilvered Fiber Reinforced Polymeric I-beams. PhD thesis, Georgia Institute of Technology, Atlanta, Georgia 2000.

15. Ascione L, Giordano A, Spadea S. Lateral Buckling of Pultruded FRP Beams. Composites Part B: Engineering 2011;42(4): 819-824.

16. Clark JW, Hill HN. Lateral buckling of beams. J Struct Div-ASCE 1960; 86(ST7):175-196.

17. Dutheil J. Verifica Delle aste Compresse: Principi Fondamentali. Construzioni Metalliche 1966 18(4): 266–275.

18. Di Tommaso A, Russo S. Shape influence in buckling of GFRP pultruded column. Journal of Mechanics of Composite Materials 2003; 39(4):329-340.

19. Lane A. An Experimental Investigation of Buckling Mode Interaction in Pultruded Fiber Reinforced Plastic Columns. PhD Thesis, University of Warwick, UK 2002.

20. Abaqus. 'User Manual, version 6.10,' Hibbitt, Karlsson and Sorensen, Inc 2011.

21. Tomblin J, Barbero E. Local Buckling Experiments on FRP Columns. Thin-Walled Structures 1994;18(2): 97-116.

22. Bank LC. Shear Properties of Pultruded Glass Fiber Reinforced Plastic Materials. Journal of Materials in Civil Engineering 1990;2(2): 118-122.

23. Sonti SS, Barbero EJ. Material Characterization of Pultruded Laminates and Shapes. Journal of Reinforced Plastics and Composites 1996;15(7): 701-717.

24. Zureick A, Scott D. Short-Term Behavior and Design of Fiber-Reinforced Polymeric Slender Members under Axial Compression. Journal of Composites for Construction 1997;1(4): 140-149.

25. Steffen RE. Behavior and Design of Fiber-reinforced Polymeric Composite Equal-leg Angle Struts. PhD thesis, Georgia Institute of Technology, Atlanta, Georgia 1998.

26. Turvey GJ. Torsion Tests on Pultruded Glass-reinforced Plastic Sheets. Journal of Composites Science and Technology 1998;58(8): 1343-1351.

27. Roberts TM, Al-Ubaidi H. Flexural and Torsional Properties of Pultruded Fiber Reinforced Plastic I-Profiles. Journal of Composites for Construction 2002;6(1): 28-34.

28. Mottram JT. Shear Modulus of Standard Pultruded Fiber Reinforced Plastic Material. Journal of Composites for Construction 2004;8(2): 141-147.

29. Qiao PZ, Zou GP, Davalos JF. Flexural-torsional Buckling of Fiber-reinforced Plastic Composite Cantilever I-Beams. Composite Structures 2003;60(2): 205-217.

30. Shan LY and Qiao PZ. Flexural-torsional Buckling of Fiber-reinforced Plastic Composite Open Channel Beams. Composite Structures 2005;68(2): 211-224.

31. Mottram JT and Shaw CT. Using Finite elements in mechanical design. McGRAW-HILL book company europe, UK, 1996.

32. Trahair NS. Flexural-Torsional Buckling of Structures. E & FN Spon, London, UK 1993.

33. Abaqus. Theory manual, version 6.11. Hibbitt, Karlsson and Sorensen, Inc 2011.

34. Riks E. An Incremental Approach to the Solution of Snapping and Buckling Problems. International Journal of Solids and Structures 1979;15(7): 529-551.

35. Wempner GA. Discrete Approximations Related to Nonlinear Theories of Solids. International Journal of Solids and Structures 1971;7(11): 1581-1599.

36. Crisfield MAA. Fast Incremental/Iterative Solution Procedure that Handles "Snap-through". Computers and Structures 1981;13(1-3): 55-62.

37. Sapkás Á, Kollár LP. Lateral-torsional buckling of composite beams. Int J Solids Struct 2002;39(11):2939-2963.

38. Machado SP, Cortínez VH. Lateral buckling of thin-walled composite bisymmetric beams with prebuckling and shear deformation. Eng Struct 2005;27(8):1185-1196.

39. Mohri F, Azrar L, Potier-Ferry M. Lateral Post-buckling Analysis of Thin-walled Open Section Beams. Thin-Walled Structures 2002;40(12): 1013-1036.

40. Minghini F, Tullini N, Laudiero F. Buckling analysis of FRP pultruded frames using locking-free finite elements. Thin Wall Struct 2008;46(2):223-241.

41. Mottram JT, Brown ND, Anderson D. Physical Testing for Concentrically Loaded Columns of Pultruded Glass Fibre Reinforced Plastic Profile. Structures and Buildings 2003;156(2): 205-219.

42. ASTM D3917-11. Standard Specification for Dimensional Tolerance of Thermosetting Glass-Reinforced Plastic Pultruded Shapes. American Society for Testing and Materials (ASTM), West Conshohocken, PA 2011.

43. Lane A, Mottram JT. Influence of Modal Coupling on the Buckling of Concentrically Loaded Pultruded Fibre-reinforced Plastic Columns. Proceedings of the Institution of Mechanical Engineers, Part L: Journal of Materials Design and Applications 2002;216(2): 133-144.

44. Singer J, Arbocz J, Weller T. Buckling Experiments Experimental Methods in Buckling of Thin-Walled Structures: Volume I Basic Concepts, Column, Beams and Plates. John Wiley & Sons, Chichester, 1997.

45. Lee S. Flexural-torsional Buckling of Pultruded T-sections. PhD Thesis, Georgia Institute of Technology, Atlanta, Georgia 2001.

46. Afifi AAM. Buckling of Stiffened Pultruded GRP Plates and Columns. PhD thesis, University of Lancaster, UK 2007.

47. Roberts TM. Influence of Shear Deformation on Buckling of Pultruded Fiber Reinforced Plastic Profiles. Journal of Composite for Construction 2002;6(4): 241-248.

Figure caption

Figure 1. FE Cartesian coordinate system, and mesh with displacement end boundary conditions BC2 (for $k = 1$ and $k_w = 0.5$).

Figure 2. Eigenvalue analysis for initial Minor axis out-of-straightness geometric imperfection shape along the I-beam.

Figure 3. Model for 'twisting' couple applied at free ends of I-beam.

Figure 4. Initial geometric imperfection shape from pure torsion and linear elastic small displacement FEA.

Figure 5. Effect of load height on elastic critical buckling load when beam is of FRP or steel.

Figure 6. Normalized buckling load ($P_{cr,FEA}/P_{cr}$) versus slenderness ratio (L/h) for a simply supported I-beam subjected to a vertical point load at mid-span and positioned either on top flange, at the shear centre or on bottom flange.

Figure 7. Vertical load (P) with vertical deflection (w) for the PFRP beam, having span of two metres and load applied at either Top flange, Shear centre or Bottom flange.

Figure 8. Influence of end warping fixity boundary condition on LTB resistance.

Figure 9. Load (P) and vertical displacement (w) for the FRP beam at 2.0 m span having an initial Minor axis out-of-straightness deformation from $L/10000$ to $L/240$.

Figure 10. Illustration to show the secant stiffness reduction method to establish the limiting buckling load when imperfections negate a bifurcation buckling failure.

Figure 11. Influence of magnitude of initial geometric imperfections on LTB resistance of a pultruded beam of size 101.6×50.8×6.4 mm at span of 1.0 m.

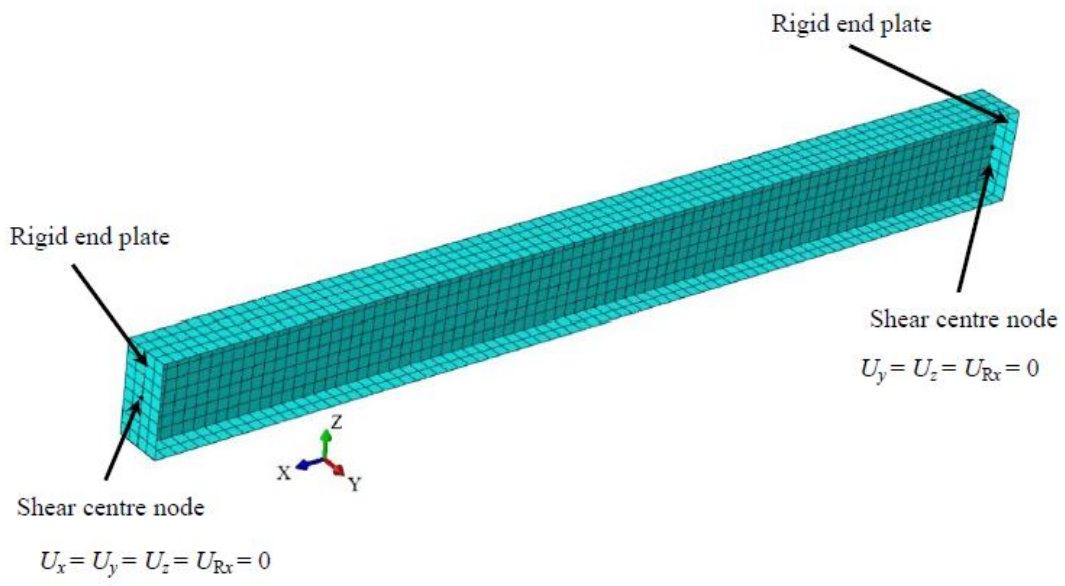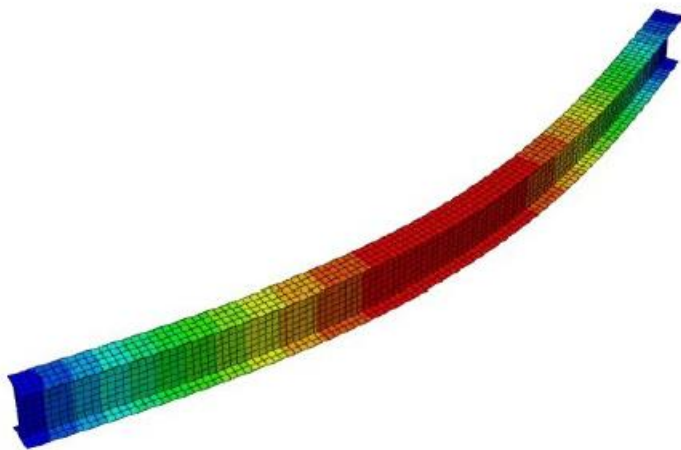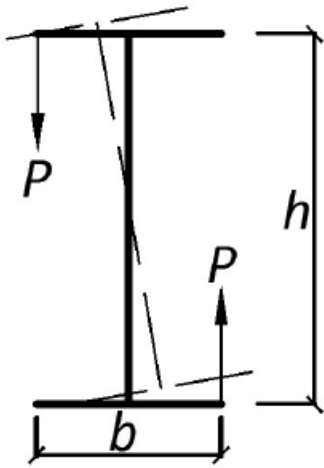Figure 12. Influence of having constant geometric imperfections and varying beam span from 1.0 to 4.0 m.
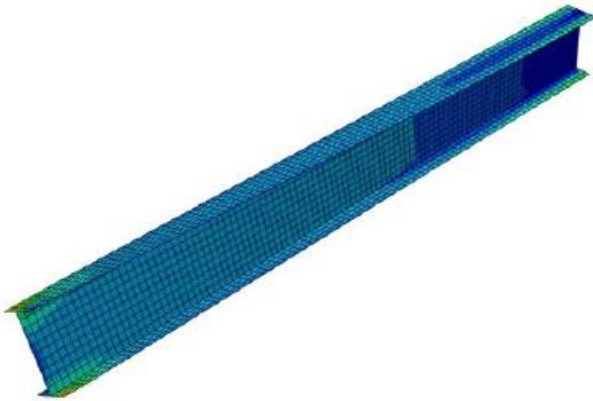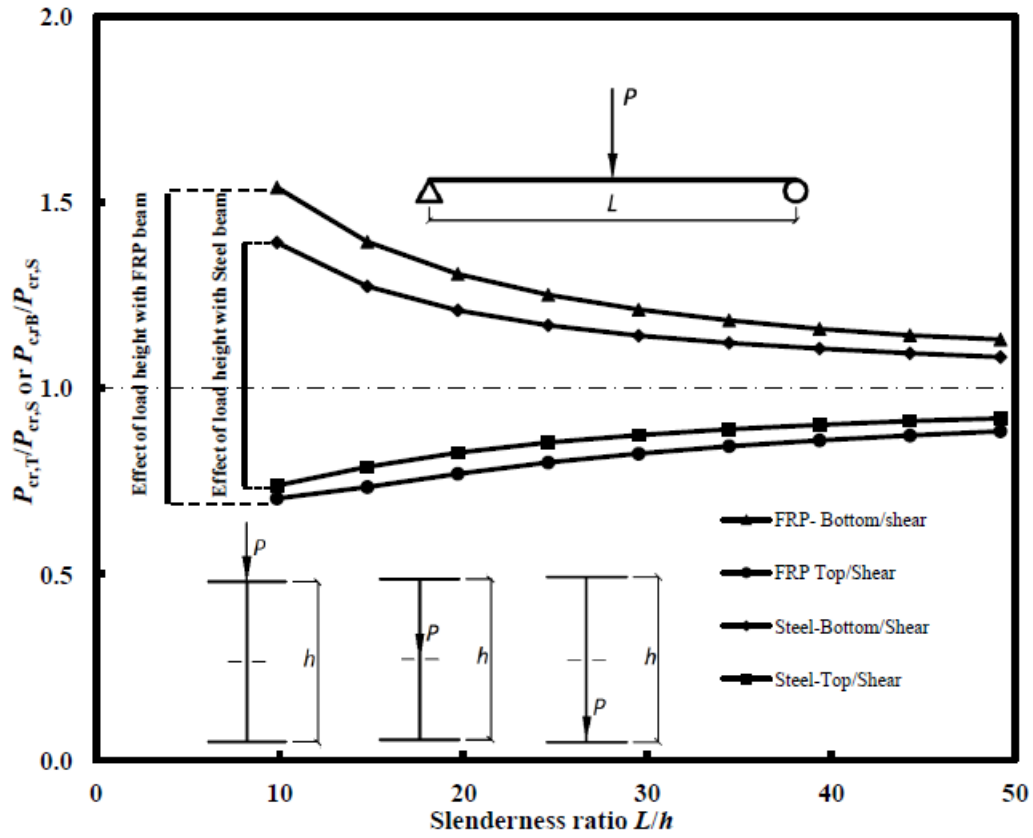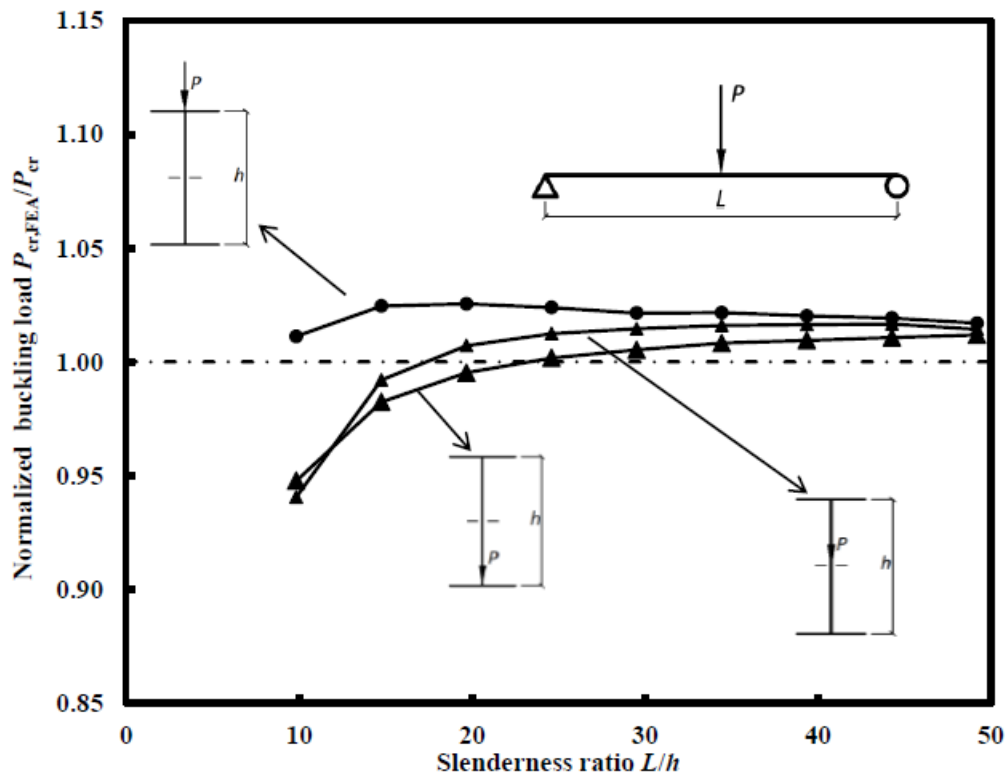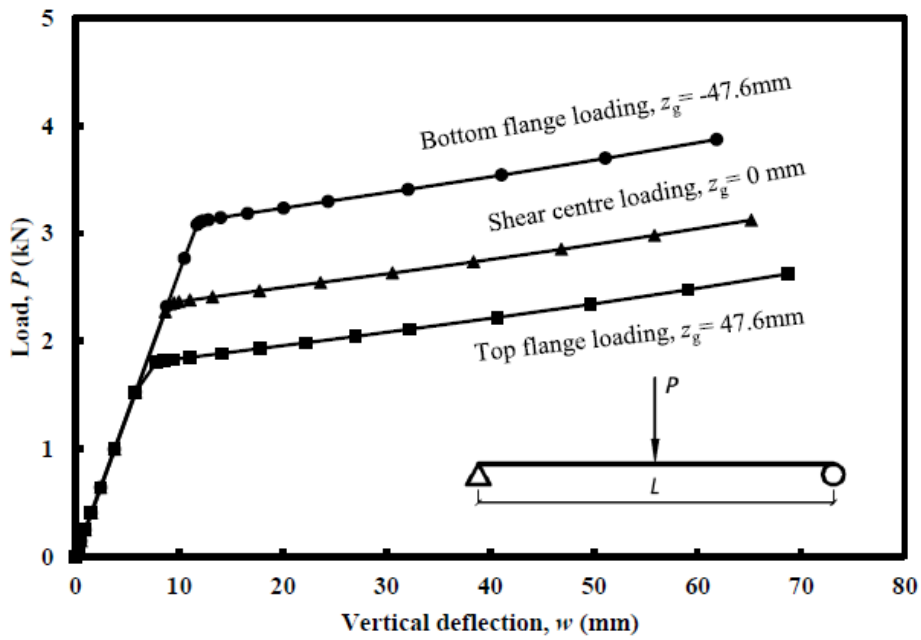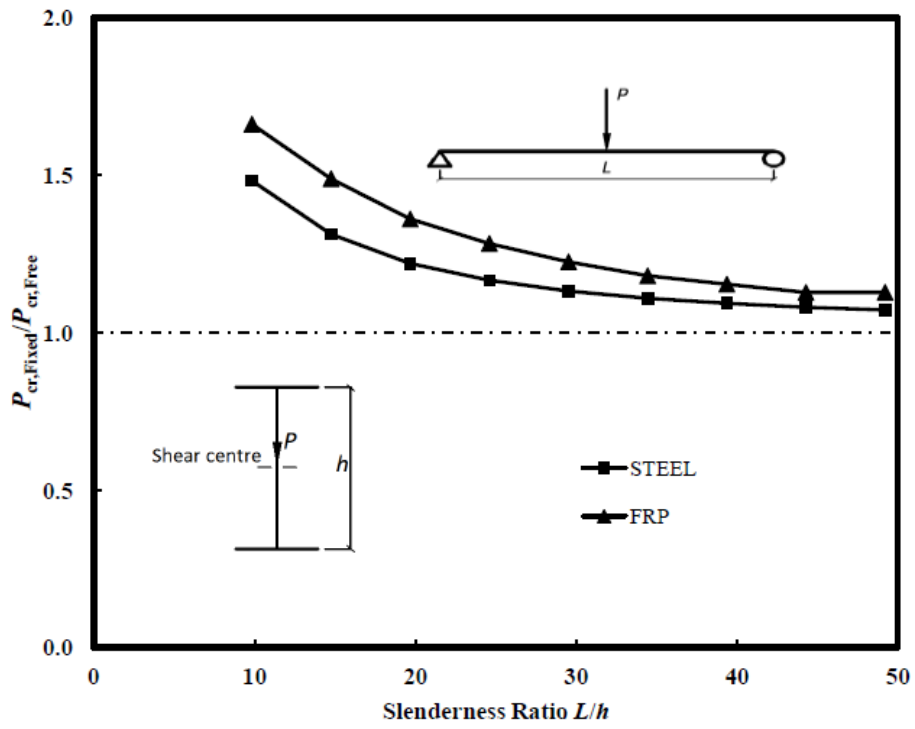
Figure 1

Figure 2

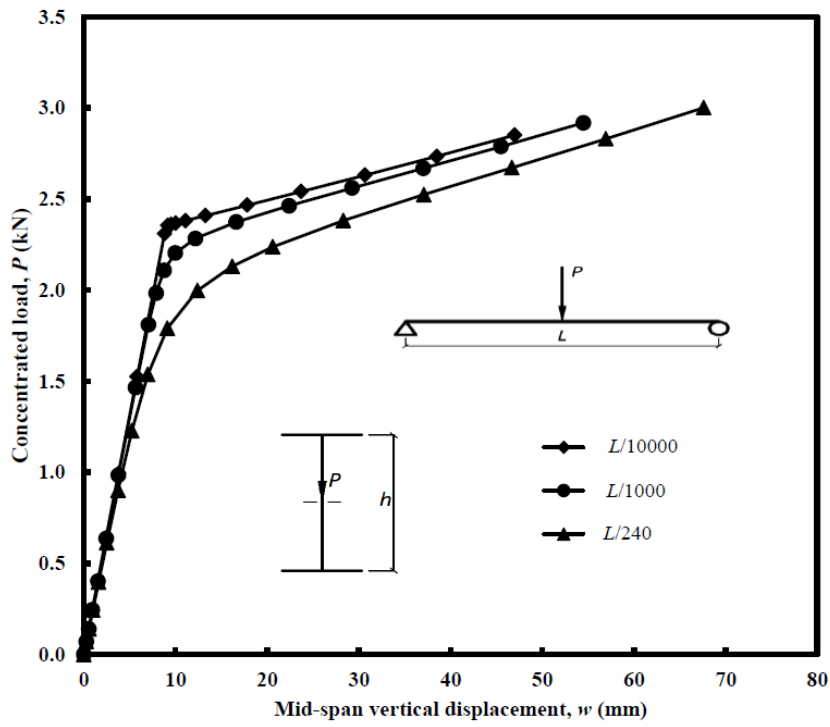Figure 3

Figure 4
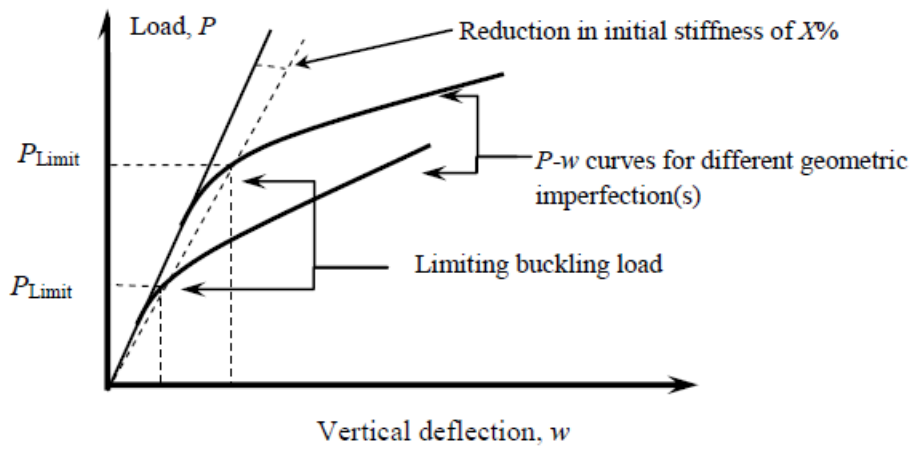
Figure 5
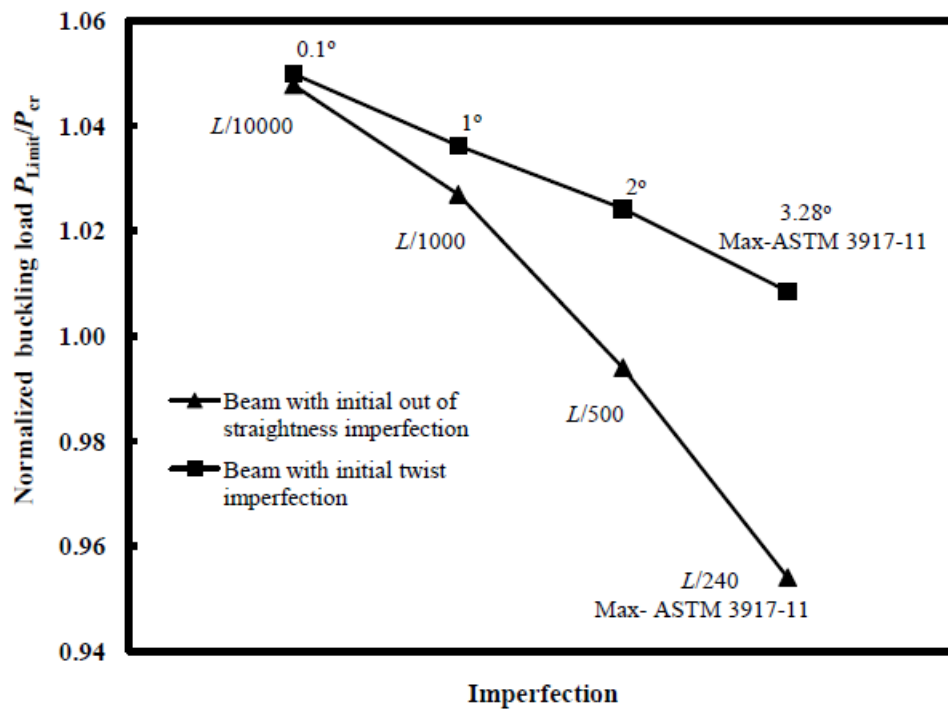
Figure 6

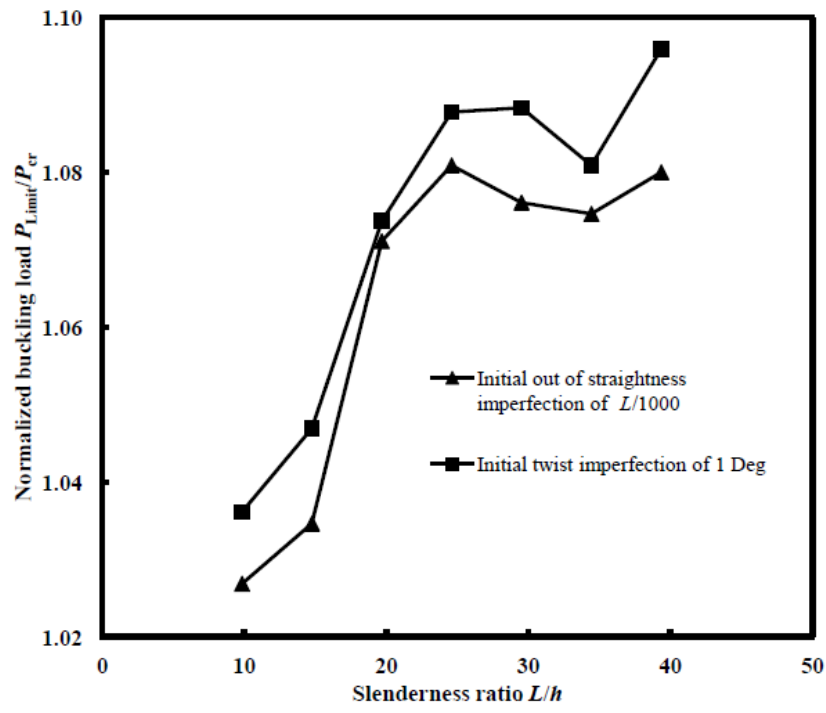

Figure 7

Figure 8

Figure 9

Figure 10

Figure 11

Figure 12

Table 1. Previous test or micromechanical values for the in-plane shear modulus (G_{LT}) of PFRP material in standard shapes.

Author(s) or pultruder's design manual	In-plane shear modulus, G_{LT}		
	kN/mm^2	Test or prediction method	Pultruder
(1)	(2)	(3)	(4)
Strongwell [2]	Null		
Creative Pultrusion Inc [3]	2.9	Full-section	Creative Pultrusions Inc.
Bank [22]	2.4-2.8	Isopescu	Creative Pultrusions Inc.
Sonti and Barbero [23]	3.9-4.5	Isopescu and Torsion	Creative Pultrusions Inc.
Zureick and Scott [24]	4.1-4.8	Isopescu	Strongwell
Steffen [25]	3.5-4.5	Modified (Isopescu) V-notched beam	Strongwell
Turvey [26]	3.0-3.6	Torsion	Strongwell
Roberts and Al-Ubaidi [27]	4.4-4.9	Torsion	Fiberforce Composites
Lane [19]	3.2-3.7	Resin burn-off and Micromechanical modelling	Creative Pultrusions Inc.

Table 2. Elastic critical buckling load for lateral-torsional buckling with mesh refinement.

Shell element side lengths (mm)	Number of elements per metre	Elastic critical buckling load, $P_{cr,FEA}$ (kN)
25.4	280	11.0
12.7	1108	9.96
8.5	2478	9.95
6.4	4368	9.95
5.1	6860	9.95

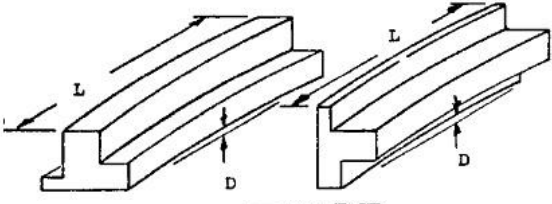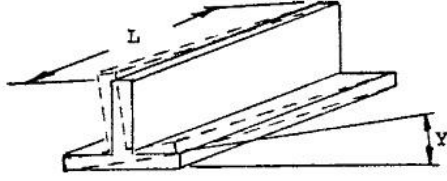Table 3. Allowable deviation from straightness and twist according to Tables 3 and 4 in standard ASTM D3917-11.

Type of imperfection	Illustration of geometric tolerance	Allowable deviation from straight
(1)	(2)	(3)
Out-of-straightness		$D = 4.167$ x L (length in meters)
Twist		$Y/L = 3.281$ degree / m

Table 4. Measured initial geometric imperfections for pultruded standard shapes.

Author(s)	Structural shape	Maximum imperfection in terms of length L

(1)	(2)	(3)
Brooks and Turvey [10]	I	Out-of-straightness for flanges and web is L/900.
Zureick and Scott [24]	I and box	Out-of-straightness of: I-beam lies between L/812 to L/1835; Box lies between L/1103 to L/8053. Maximum did not always exist at mid-span.
Mottram *et al.* [41]	Wide flange I	Maximum out-of-straightness is L/4500.
Lane and Mottram [43]	Wide flange I	Minor-axis out-of-straightness is L/3200.

Table 5. Vertical deflection (w) with vertical load (P) at 2 m span with out-of-straightness geometric imperfection of L/10000 (see Figure 9).

Load P (kN)	Deflection w (mm)	Secant stiffness P/w (kN/mm)
(1)	(2)	(3)
0.070	**0.267**	**0.262**
0.140	0.534	0.262
0.245	0.934	0.262
0.403	1.53	0.262
0.639	2.44	0.262
0.993	3.79	0.262
1.53	5.81	0.262
2.31	8.80	0.262
2.35	9.18	0.256
2.36	9.53	0.248
2.37	10.0	0.236
2.38	11.1	0.215
2.41	13.3	0.182
2.47	**17.8**	**0.138**
2.54	23.7	0.107
2.63	30.7	0.086
2.73	38.5	0.071
2.85	47.0	0.061
2.98	56.0	0.053